Ab initio molecular dynamics (AIMD) simulations of NaCl, UCl_3 and NaCl-UCl_3 molten salts

XXX

Abstract

Ab initio molecular dynamics (AIMD) simulations are used to calculate select thermophysical and thermodynamic properties of NaCl, UCl_3 and NaCl-UCl_3 molten salts. Following established approaches, the AIMD simulations include a model for Van der Waals interactions. The Langreth & Lundqvist, DFT-D3 and dDsC dispersion models are first tested for molten NaCl in order assess their accuracy for density and heat capacity predictions across a range of temperatures. Based on the NaCl results, the Langreth & Lundqvist and dDsC methods are extended to the UCl_3 system and compared to available experimental data. Next, mixtures of NaCl-UCl_3 are investigated and analyzed with respect to the deviation from ideal solution behavior. For the dDsC simulations, density deviates by up to 2% from an ideal mixture, with the maximum occurring close to the eutectic composition, possibly shifted slightly towards the NaCl rich side. The temperature dependence of the deviation from ideal solution is weak in the NaCl rich region, but more discernible in the UCl_3 rich region. The mixing energy also deviates from an ideal solution and exhibits a minimum of about -0.07 eV per formula unit, again close to the eutectic composition, but this time shifted slightly towards the UCl_3 rich region. Within the uncertainty of the simulations, the mixing energy does not depend on temperature. The trends observed for mixing properties are rationalized by correlating them to the coordination chemistry, which emphasizes the competition between increasing the Cl coordination around U ions and maintaining the extended network formed by U and Cl ions as the NaCl concentration increases. The density and mixing energy predictions are also compared to existing experimental measurements.

1. Introduction

Molten salt reactors (MSRs) are among the advanced concepts pursued under the generation IV nuclear energy technology umbrella. However, the basic concept is not new and was first developed as part of the effort to power aircrafts with nuclear energy in the 1950's. Later in the 1960's, Oak Ridge National Laboratory (ORNL) built and operated the Molten-Salt Reactor Experiment (MSRE) [1]. This reactor used a fluoride salt with uranium as fuel. Fluoride salts are still highly relevant and proposed in several designs. In addition, chloride salts are being considered for MSRs operating in the fast neutron spectrum. The present study focuses on chloride salts, in particular the NaCl-UCl_3 system, which is one of the primary fuel salt candidates.

Experimental characterization of UCl_3 densities have been reported by Janz et al. [2] and Desyatnik et al. [3]. The density correlations derived from these two experimental data sets deviate significantly from each other. Desyatnik et al. [3] also investigated the density of NaCl-UCl_3 mixtures. They identified a negative deviation from an ideal solution across most of the composition range, with the high-temperature UCl_3 rich region deviating slightly from this trend. Maatsura et al. [4] measured the mixing energies of NaCl-UCl_3 at 1173 K, which highlighted a negative deviation from ideal solution behavior (exothermic reaction) with a minimum of -0.07 to -0.08 eV per formula unit close to the eutectic composition ($x \approx 0.35$, where x is the UCl_3 fraction), but perhaps slightly shifted towards the 50-50 composition. There are two Calphad assessments of the NaCl-UCl_3 system [5, 6]. The magnitude and shape of the NaCl-UCl_3 mixing energies are noticeably different between the two assessments [6]. The assessment by Benes et al. [5] arrived at a form with a minimum close to the eutectic composition, while Yin et al. [6] used the experimental data due to Matsuura et al. [4] as input, which resulted in a more negative mixing

energy that is shifted slightly closer to the 50-50 composition. The magnitude of the mixing energy is off by about 50% between the two assessments.

The sparse and sometimes contradictory experimental data on molten salts in general and the NaCl-UCl_3 system in particular provide justification for pursuing modeling and simulations as a complementary approach to gain improved understanding. This opportunity is already acknowledged in the literature. Molecular dynamics simulations based on both classical potentials and AIMD simulations have been used to study chloride salts involving actinides [7–10]. Li et al. [7] used AIMD simulations to study the local structure of UCl_3, UCl_4 and mixtures of UCl_3, UCl_4 and NaCl at 1173 K. This study showed good agreement with experiments for the radial distribution function of the first coordination shell and identified network formation of UCl_3 units in mixed NaCl-UCl_3 salts [7]. In order to study temperature dependent thermophysical properties, a semi-empirical potential was developed [8]. This potential successfully predicted density, thermal conductivity and viscosity, though validation is challenged by the lack of experimental data. Nam et al. [9] studied the solution thermodynamics of dilute concentrations of UCl_3 in a base salt and investigated the properties of base salts for different Van der Waals interaction models. Song et al. [10] performed AIMD simulations of densities and transport properties in a LiCl-KCl eutectic salt with a small concentration of UCl_3.

In the present study, AIMD simulations relying on different models for the Van der Waals interactions were used to predict temperature dependent thermophysical (density) and thermochemical (mixing energy and heat capacity) properties of NaCl, UCl_3 and NaCl-UCl_3. The standard PBE exchange-correlation potentials typically used were extended to include a Hubbard U model for the actinide 5f electrons. The purpose of the study was first to determine with what accuracy fundamental properties can be predicted with AIMD simulations for actinide containing salts, second to populate some of the data gaps that exist in the literature and third to provide understanding of the link between coordination chemistry and properties.

This paper is organized as follows. The methodology is described in Sec. 2, followed by results and discussion in Sec. 3. First, the benchmark for NaCl is presented, after which the UCl_3 results are reviewed followed by NaCl-UCl_3 mixtures. The implications of our results are discussed in Sec. 4 and, finally, our conclusions are presented in Sec. 5.

2. Methodology

The AIMD simulations were performed with the VASP code [11]. The simulations used a range of supercell sizes with the largest consisting of 216 (NaCl), 216 (UCl_3) and 134-184 (NaCl-UCl_3 mixtures) atoms. The smallest cells for the same systems contain 64, 64 and 60-72 atoms, respectively. Further details will be provided in Sec. 3. For NaCl and UCl_3 the supercells were created by expansion of the crystalline unit cells followed by melting of the lattice by performing high temperature MD simulations. The mixed supercells were created by replacing Na ions with U ions or vice versa, in some cases additional molecular units were added to ensure that a suitable number of atoms were maintained in the supercells. In some cases the PACKMOL package followed by high temperature annealing were used for generation of supercell structures.

The differently sized supercells were investigated in order to understand and optimize the compromise between computational efficiency, enabling sampling in the time domain, and accuracy with respect to long range interactions. The radial distribution function (RDF) was used as the most basic measure of the adequacy of the supercell size, with convergence with respect to the targeted thermophysical and thermodynamic properties following suite. All the supercells investigated properly capture the expected radial distribution function in the liquid state. This behavior is exemplified in Figures 1a) and 1b) for UCl_3 and NaCl supercells of different size, respectively. The smaller cells predict essentially identical radial distribution functions as compared to the larger cells, but enable improved computational efficiency. Although the larger cells may still be more accurate for, e.g., mixed salts exhibiting more complex radial distribution functions, the situation in mixed salts is further complicated by the need to sample sufficient configurations to resolve the preferred short and intermediate range distribution of ionic species in network forming salts such as UCl_3 [7]. This requires fairly long simulation times. Proper sampling is easier to achieve in smaller supercells given the computational cost of AIMD simulations, even though the radial distribution itself, as well as other properties, may be better described in a larger supercell. For this reason, our production runs tend to use supercells of intermediate size. Based on the verification against large

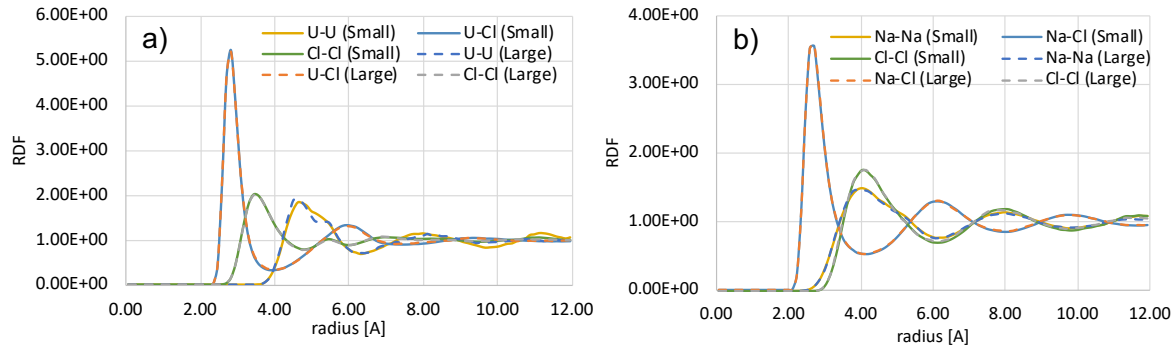

Figure 1: The predicted radial distribution function in a) UCl_3 and b) NaCl obtained by supercells containing 64 (small) and 216 (large) atoms at 1250 K.

supercells for the radial distribution function above and further examples in Sec. 3, the results in the present study are considered sufficiently converged with respect to supercell size.

All simulations used the Γ point for integration in reciprocal space. The accurate simulation setting was utilized in VASP, but the plane wave cut-off energy was increased above the standard setting to 400 eV. Gaussian smearing with a smearing parameter of 0.05 eV was used for the partial occupancies of the wave functions. The convergence criteria for the electronic minimization was at least 10^{-3} eV for NaCl and 5×10^{-3} eV for salts containing uranium. Further details to be added.

The Projector Augmented Wave (PAW) method was used to describe the core electrons [12, 13]. The PAW potentials supplied with VASP for the PBE exchange-correlation potential were utilized. For Na, the version that only includes the s electron(s) in the valence shell was used for some of the simulations. Further details to be added. The PAW potential for Cl also included p electrons and for U it included the outer s, p and f electrons in the valance shell.

Calculations for U ions were performed with a Hubbard U term included for the 5f electrons, in order to capture the impact of strong electron correlations. The Lichtenstein approach [14] was used for the Hubbard U methodology. Further details to be added. An approximate U value range of 3.2-4.2 eV was determined by using scoping constrained DFT linear-response method for crystalline UCl_3 [15]. These values are similar to those proposed for UO_2 [16]. After confirming that the values for UCl_3 were close to those for UO_2, the values for UO_2 were adopted in the present study ($U = 4.5$ eV and $J = 0.51$ eV, yielding $U - J = 3.99$ eV). Future work may consider further optimization of the Hubbard U (and J) parameters, but the results and conclusions are not expected to significantly change based on this choice, as long as the value is sufficiently large to ensure an insulating ground state. It should be noted that the effective U value depends on the coordination environment and consequently could differ between crystalline UCl_3 and molten salts. It could also be a function of time in the simulations as the environment may change. Future work may consider these questions in more detail, but it is beyond the scope of the present study. The effect of the Hubbard U parameter for molten uranium chloride salts is the same as for crystalline UO_2; without the U parameter the salts are predicted to be metallic, which is contrary to the expected behavior, see Fig. 2. Even though useful results may certainly be obtained while ignoring the strong correlations captured by the Hubbard U model and accepting the resulting metallic character predicted for the salts, there are limitations to this approach. For reference, a few simulations were performed without the Hubbard U model.

A uranium ion in its 3+ state has a localized magnetic moment. In order to mimic the disordered arrangement of magnetic moments expected at temperatures where the salts are molten, the spins were arranged in an anti-ferromagnetic (AFM) pattern and then allowed to relax during the simulations. In the context of molten salts, the AFM option is similar to a random distribution with a total magnetic moment in the supercell close to zero. The predicted properties are not strongly influenced by the magnetic ordering. Further details to be added.

It is well-established in the literature that Van

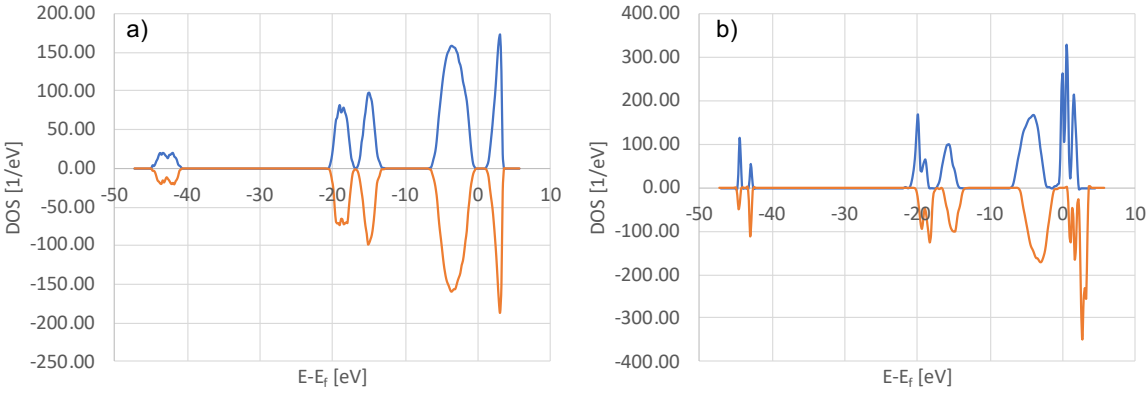

Figure 2: The predicted density of states for simulations of molten UCl_3 at 1250 K, a) including (AFM) and b) not including (FM) a Hubbard U model. Furhter details to be added.

der Waals or dispersion interactions are critical for reproducing the density of molten salts by DFT methods [7, 9, 17]. Previous simulations have used both the DFT-D3 [7, 18] and the Langreth & Lundqvist [9, 19, 20] methodologies for various molten chloride salts. Both methods were used in the present study. In addition, the density-dependent energy correction (dDsC) method [21, 22] was used with the goal of improving accuracy. The dDsC method does not include parameters for f elements in the standard VASP version. In order to enable simulations the corresponding parameters were taken from Ref. [23].

The AIMD simulations for the molten salt supercells were performed using isobaric (NPT) conditions. The primary intent of the NPT simulations (with the pressure set to zero) is to evaluate density, thermal expansion, heat capacity and mixing energy. All NPT ensemble simulations used the the Langevin thermostat in VASP. For the NPT simulations, the temperature friction coefficient was set to 10 ps^{-1} and the friction coefficient for the lattice degrees of freedom to 1 ps^{-1}. The time step was set to 2 fs for production runs between ~1000 K and 1500 K. Around and below 1000 K a larger time step, up to 5 fs, is warranted due to the slow dynamics of uranium ions. Further details to be added.

The simulations used pre-equilibrium and equilibration runs that involve melting the lattice and ensuring convergence of the total energy and pair distribution function for the temperature of interest. After pre-equilibration and equilibration, production runs follow for at least 20 ps. Some simulations used longer production runs, in particular this applies to the simulations based on smaller supercells (up to 50 ps) and systems containing a mixture of UCl_3 and NaCl (up to 40 ps). NPT simulations require long equilibration runs and may sometimes leave the equilibrium state due to distortions of the supercells, which is in part a consequence of applying the technique to somewhat small supercells. All simulations were inspected to avoid sampling such regimes. Further details to be added.

Properties were calculated by averaging over the production run (not including the equilibration or pre-production time). Densities were trivially obtained from the supercell volume and heat capacities from the slope of the total internal energy (E_{tot}) as function of temperature.

$$C = \frac{\partial E_{tot}}{\partial T} \tag{1}$$

For the NPT ensemble, this corresponds to heat capacity at constant pressure (C_p). Mixing energies were calculated from the potential energy (E_{pot}) of the mixed salt with pure NaCl and UCl_3 at the same temperature as the reference.

$$\begin{aligned} E_{mix} = E_{pot}(U_x Na_y Cl_{3x+y}) - \\ -xE_{pot}(UCl_3) - yE_{pot}(NaCl). \end{aligned} \tag{2}$$

Further details to be added.

3. Results

3.1. AIMD simulations of NaCl

3.1.1. Density and structure

Figure 3a plots the predicted density of molten NaCl as function of temperature for the DFT-

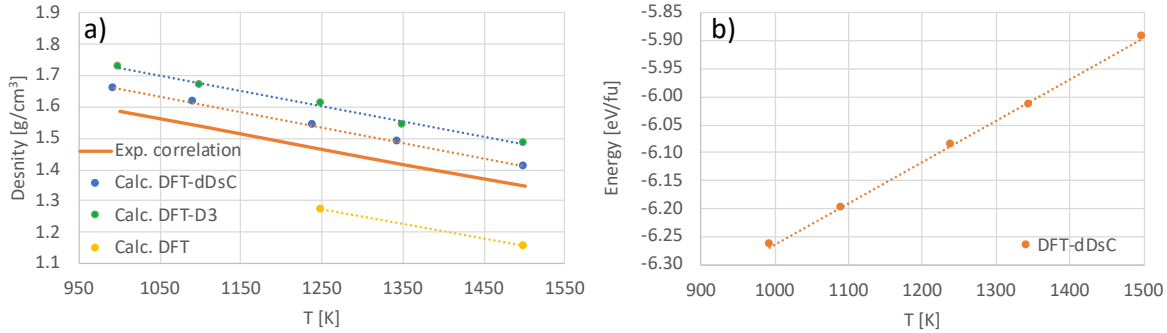

Figure 3: a) Density of NaCl predicted with two different models for dispersion forces (D3 and dDsC) and one without (small cell witih 64 atoms for dDsC, large cell with 208 atoms for others). Experimental data is represented by the correlation plotted as an orange line [2]. b) Calculated total energy of NaCl as function of temperature (small cell). The line is a least-squares fit to data points and the slope represents the heat capacity.

D3 and DFT-dDsC Van der Waals models as well as simulations without any dispersion interaction. The results refer to the supercell size that we consider best converged for each methodology, see caption and below for further discussion. A correlation derived from experimental data is also shown [2]. All simulations reproduce the temperature dependence of the density obtained from experiments. However, as expected, only the simulations that account for dispersion interactions are within 10% of the experimental density correlation. The best agreement is obtained for the dDsC dispersion model, which is within 5% or less of the experimental correlation across an extended temperature range. The calculated (dDsC) correlation for the density as function of temperature is listed in Table 1. The radial pair distribution function at 1250 K is reported in Figure 1, which highlights first, second and third-shell coordination distances of 2.70 Å, 3.78 Å and 4.14 Å, respectively. The predicted pair distribution function is in good agreement with experimental values [24]. Further details to be added.

3.1.2. Heat capacity

Figure 3b plots the total energy per formula unit of molten NaCl as function of temperature. The derivative equals the heat capacity of NaCl, which is also tabulated in Table 1 together with an experimental reference value [25]. The results refer to the supercell size that we consider best converged for each methodology, see caption and below for further discussion. The simulation results indicate a constant heat capacity, though in order to identify small deviations from this behavior a denser temperature mesh would be required. The good agreement between simulations and experiments for the heat capacity (see Table 1) further emphasizes the accuracy of the AIMD simulations. Further details to be add.

Further details to be added.

3.1.3. Impact of supercell size and other simulation settings

The results in Figure 3 refer to simulations based on the supercell that we consider best converged. Figure 4 compares these results with those obtained from other supercells. Given the good agreement between the results from different supercells, density and heat capacity are considered accurately

	Density (g/cm^3)	Heat capacity (J/mol/K)
NaCl Calculated (dDsC)	$2.1594 - 0.0004993T$	71.6
NaCl Experiment	$2.061 - 0.0004759T$ [2]	66.9 [25]
UCl_3 Calculated (dDsC)	$6.1066 - 0.001383T$	145.3
UCl_3 Experiment	$6.375 - 0.001522T$ [3]	150 [5],129.704 [6]

Table 1: Calculated and experimental correlations and values for density and heat capacity of NaCl and UCl_3.

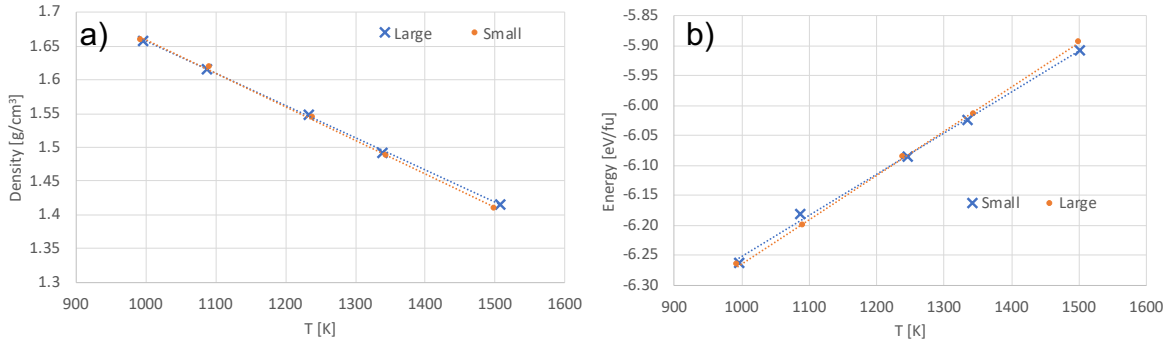

Figure 4: a) Calculated density and b) total energy of NaCl as function of temperature for the large and small supercells. The lines are least-squares fits to data points and the slope represents the heat capacity.

represented by all supercell sizes that were investigated. These results suggest that for NaCl, the larger supercells are not required to achieve converged results for density and heat capacity, which is consistent with the discussion of radial distribution functions in Sec. 2. The small variations between supercells are more likely related to sampling differences, rather than due to the supercell size. Consequently, the converged results in Figure 3 as well as the correlations in Table 1 are representative of all simulation results in this study, regardless of the supercell size. Further details to be added.

3.2. AIMD simulations of UCl_3

3.2.1. Density and structure

Following the results for NaCl, the best performing Van der Waals model (dDsC) was applied to UCl_3. Further details to be added.Figure 5a) plots the predicted density for UCl_3 as function of temperature for the dDsC dispersion model. These results refer to the supercell size that we deem to be best converged and most representative of the UCl_3 system, see below for further discussion. The figure also compares the predicted densities to two literature correlations derived from experiments [2, 3]. The two experimental correlations for density are surprisingly different and cannot both be correct, except in a narrow temperature range. The temperature dependence is predicted to be close to linear across the full temperature range investigated and agrees very well with the experimental data due to Desyatnik et al. [3]. Further details to be added. The densities in Figure 5 were fitted to linear correlations and summarized in Table 1.

The radial pair distribution function at 1250 K is reported in Figure 1, which highlights a first-shell coordination distance of 2.82 Å. The coordination distance is in excellent agreement with the experimental values of 2.82 Å [26] and 2.84 Å [27] measured at 1113 K and 1200 K, respectively, while it is higher than the AIMD simulations by Li et al. [7], which can likely be ascribed to the application of the Hubbard U methodology in the present study. The predicted coordination numbers are within the 6 to 8 range reported in experiments and previous simulations [7, 26, 27].

3.2.2. Heat capacity

Figure 5 plots the total energy as function of temperature, from which the heat capacity can be derived by calculating the slope. The total energy closely follows a linear relation as function of temperature and, consequently, the heat capacity can be approximated as a constant in the temperature range investigated. In order to resolve small deviations from the linear relation, a denser temperature mesh would have to be used. Experimental data for the heat capacity of UCl_3 has not been identified, but our results compare very well with the value derived from the CALPHAD assessment of the UCl_3 thermodynamics due to Benes et al. [5], while it deviates somewhat from the assessment due to Yin et al. [6] (see Table 1).

Further details to be added.

3.2.3. Impact of supercell size and other simulation settings

The results discussed above for UCl_3 refer to simulations using the supercell size that we deem to be best converged and most representative of the UCl_3 system for each simulation methodology. Select results obtained from different supercell sizes

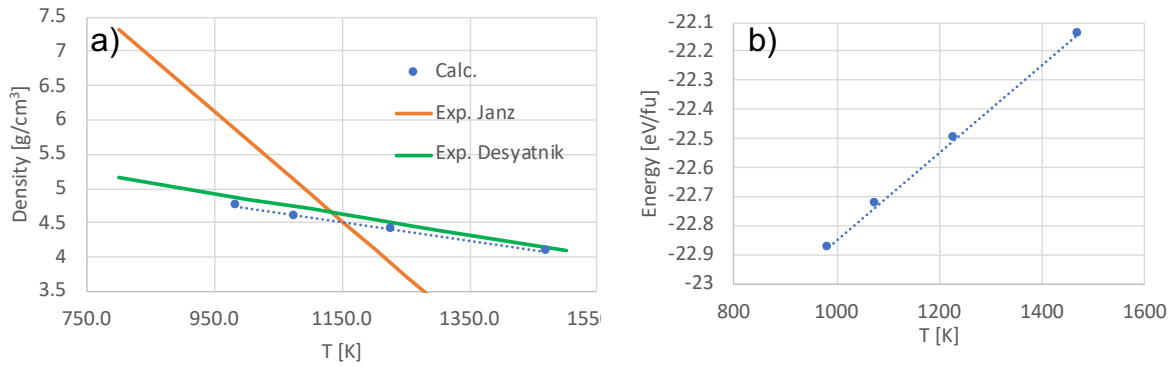

Figure 5: a) Density of UCl_3 predicted the dDsC model for the dispersion forces (small cell with 64 atoms). Experimental data is represented by the correlations plotted as green [3] and orange lines [2]. The dashed line is a least-squares fit to the calculated data points, the equations of which are summarized in Table 1. b) Calculated total energy of UCl_3 as function of temperature (small cell). The line is a least-squares fit to data points and the slope represents the heat capacity.

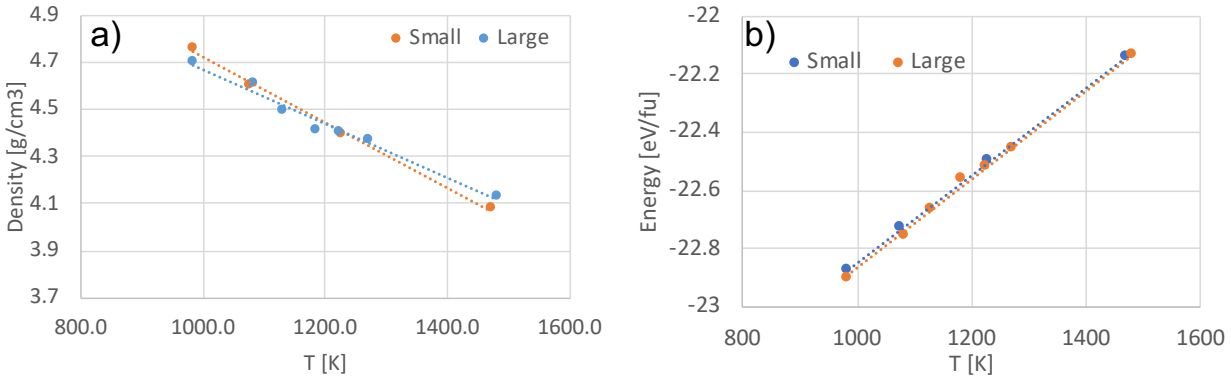

Figure 6: Calculated density and total energy of UCl_3 as function of temperature for the large and small supercells. The line is a least-squares fit to data points and the slope represents the heat capacity.

are compared in Figure 6, which exhibits fairly good agreement with each other. Any difference between supercell sizes is primarily ascribed to sampling appropriate configurations rather than an effect of increasing the numbers of ions in the simulation box, although additional simulations would be required to fully certify this conclusion. Compared to NaCl it is much more challenging to reach long simulation times for the large UCl_3 simulation cells.

3.3. Ab initio molecular dynamics simulations on NaCl-UCl_3

3.3.1. Density and structure

The density of NaCl-UCl_3 mixtures were calculated for the dDsC dispersion model at three or four (depending on composition) different temperatures between 800 K and 1500 K, as shown in Figure 7a). This figure also includes densities at the same temperatures as those of the simulations obtained from correlations derived from experimental data due to Desyatnik et al. [3]. The simulated data points are within a few per cent of the experimental data. Figure 7b) highlights the fractional deviation from ideal solution behavior as calculated from simulations and experiments [3]. It is challenging to converge the density for mixed salt solutions to an accuracy better than around one per cent of the absolute density using AIMD simulations, which gives rise to some scatter in the data points. Nevertheless, a few trends are discernible from Figure 7. The simulations suggest a negative deviation from an ideal solution (lower density than predicted by an ideal solution behavior) by up to 2-3%, except close to pure UCl_3 at high temperature

where a positive deviation is observed. According to our simulations, the magnitude of the deviation from ideal solution behavior is a function of composition and varies some with temperature starting at $x \approx 0.35$ and continuing in the UCl_3 rich composition range, while it is almost independent of temperature in the NaCl rich range. The maximum deviation from ideal solution behavior occurs close to the eutectic composition of 35% UCl_3, perhaps slightly shifted towards the NaCl rich side but it is hard to draw a solid conclusion due to uncertainties in the simulated data. These predictions are qualitatively similar to the correlations derived form experiments by Desyatnik et al. [3], though the experimental correlations predict a larger magnitude for the deviation from an ideal solution and also exhibit a stronger temperature dependence than the simulations. further details to be added.

Figure 8a) plots the density as function of temperature for each composition, which emphasizes a close to linear temperature dependence, similar to the pure end-members. The coefficients describing the linear dependence on temperature for each composition are plotted in Figure 9a). Although there is some scatter, a weak non-linear dependence on composition for both the linear and constant term (not shown) is identified. The non-linear dependence is most pronounced in the UCl_3 rich range. The density correlations identified in Figures 8a) and 9a) can also be expressed in a combined composition-temperature dependent correlation:

$$\rho(x,T) = \frac{M_{NaCl}(1-x) + M_{UCl_3}x}{\frac{M_{NaCl}(1-x)}{\rho_{NaCl}} + \frac{M_{UCl3}x}{\rho_{UCl_3}}} + \\ +e_1 + e_2T + (f_1 + f_2T)x + (g_1 + g_2T)x^2 + \\ +(h_1 + h_2T)x^3 + (i_1 + i_2T)x^4 + (j_1 + j_2T)x^5, \quad (3)$$

where the first term represents the density of an ideal solution and the subsequent terms the deviation from ideal solution behavior. M_{NaCl} and M_{UCl_3} are the molar masses of the end member salts, ρ_{NaCl} and ρ_{UCl_3} the temperature dependent densities of the end-member salts, which are taken from the correlations previously derived, T is temperature and x is the mole fraction of UCl_3 in the mixture. A least-squares fit of the coefficients describing deviation from an ideal solution are collected in Table 2.

3.3.2. Mixing energy and heat capacity

The mixing energies of NaCl-UCl_3 at temperatures ranging from 1100 K to 1500 K are plotted in Figure 10a), with the NaCl and UCl_3 end members as reference points. The mixtures exhibit a negative deviation from ideal solution behavior, which implies that the solution phase is favored over a two-phase mixture of the end-points. Addition of entropy further stabilizes the mixed solution phase, as shown in Figure 10b) by adding a simple ideal solution model to the potential energy in Figure 10a). The minimum (most negative) mixing energy is between x=0.35 and x=0.5, which qualitatively mimics the results for the density, perhaps with a slight shift towards the 50-50 composition.

The mixing energy was measured at 1100 K by Matsuura et al. [4] The results are also shown in 10a) and indicate very good agreement with the simulations across the full temperature range. In addition to the experimental data points, there are two sets of thermodynamic models for the solution energy [5, 6], see Figure 10a) for the correlation from Ref. [6]. Both thermodynamic models assume the solution energy to be independent of temperature, which is in good agreement with the simulations. The model by Yin et al. [6] was derived from the experimental measurements by Matsuura et al. [4] and consequently agree similarly well with our simulation results. The model by Benes et al. [5] exhibits a smaller mixing energy than both the experimental data points and our simulations (not shown).

The total energy for each NaCl-UCl_3 composition is plotted as function of temperature in Figure 8b), from which heat capacity can be calculated as the slope, similar to the pure NaCl and UCl_3 systems. The heat capacity is approxiamtely a linear function of the salt composition, which is expected based on the lack of temperature dependence for the salt mixing energies. The negative deviation from an ideal solution seen for the mixing energy and density is not present for the heat capacity.

Based on the results for the mixing energy, the following expression may be fitted to the mixing energy as function of the composition and temperature:

$$E_{mix}(x,T) = (e_1 + e_2T) + (f_1 + f_2T)x + \\ +(g_1 + g_2T)x^2 + (h_1 + h_2T)x^3 + (i_1 + i_2T)x^4 + \\ +(j_1 + j_2T)x^5, \quad (4)$$

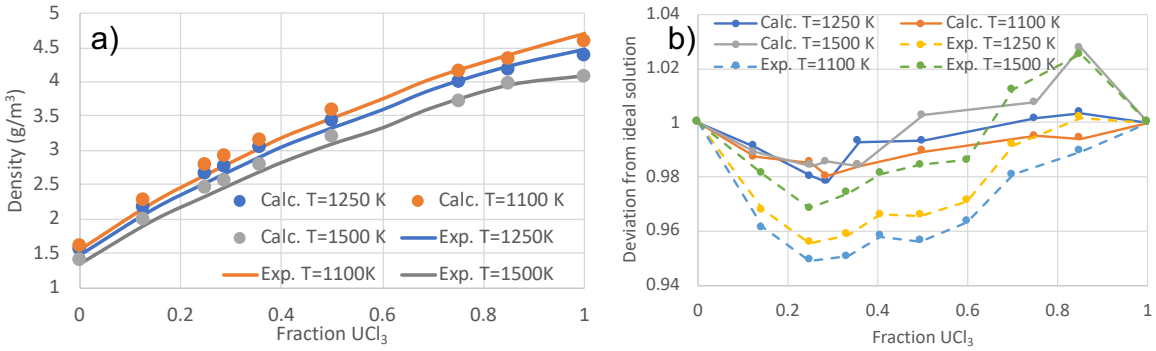

Figure 7: a) Density of NaCl-UCl_3 mixtures as obtained from simulations and experimental data [3] at temperatures between 1100 K and 1500 K. b) The fractional deviation form ideal solution behavior plotted as function of composition at temperatures between 1100 K and 1500 K.

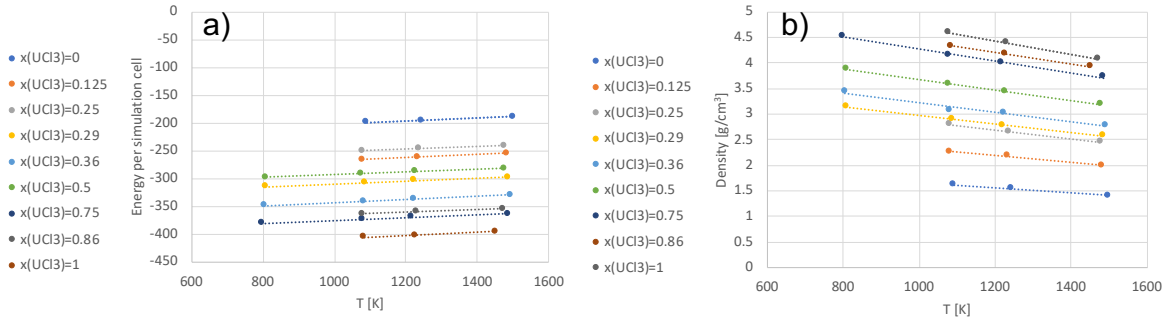

Figure 8: a) Calculated temperature dependent densities as function of composition. b) Calculated energies per simulations cell as function of composition. In both a) and b) the lines represent least-squares fits to the calculated data.

where all the temperature dependent parameters are set to zero based on the lack of disceranble temprature dependence in Fig. 10. This expression is equivalent to the Redlich-Kister expansion used in existing Calphad models. The coefficients resulting from the fit to the data in Fig. 10 are summarized in Table 2. heat capacity may be derived as the derivative of Eq. 4.

4. Discussion

This discussion section will focus on the behavior of mixed salts, in particular how the mixing properties (energy and density) relate to the evolution of the pair distribution functions in the mixed salts. Figure 11 plots the pair distribution functions at four salt compositions ($x = 0.25$, $x = 0.29$, $x = 0.36$ and $x = 0.50$) and compares them to the reference pair distribution functions for UCl_3. Ref. [7] already showed that as NaCl is added to pure UCl_3, the number of Cl ions in the first neighbor shell around U ions increases, from 6 in UCl_3 to almost 8 close to NaCl, with a corresponding decrease around Na ions. This is also confirmed in the present study (see the increase of the first peak in Figure 11 as the NaCl fraction increases). This redistribution of Cl ions clearly represents a favorable interaction as the mixing energy is negative across the full composition range. The same study also identified networks of UCl_3 units above a fractional UCl_3 concentration of 0.30, and more isolated units below this concentration. This behavior is also visi-

e_1	e_2	f_1	f_2	g_1	g_2	h_1	h_2	i_1	i_2	j_1	j_2

Table 2: A least-squares fit of the coefficients describing density of NaCl-UCl_3 mixtures as function of temperature, see Eq. 3.

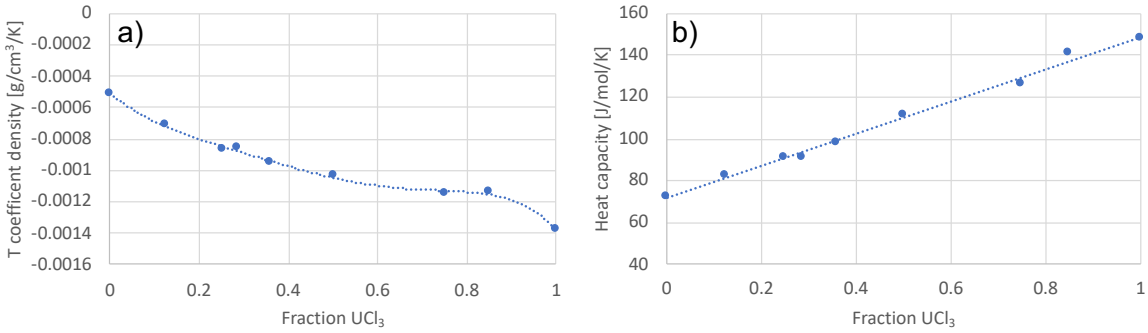

Figure 9: a) Coefficient describing the linear temperature dependence of density as function of the UCl_3 fraction. The line represents a least-squares fit of a fifth order polynomial. b) Heat capacity as function of the UCl_3 fraction. The line represents a least-squares fit of a linear correlation.

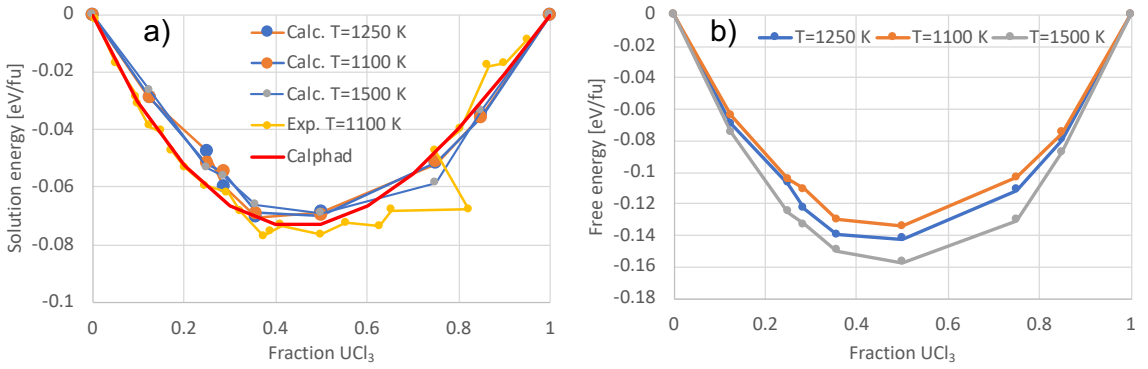

Figure 10: a) Mixing energies for NaCl-UCl_3 at 1100, 1250 and 1500 K. Pure NaCl and UCl_3 are used as references. The calculated results are compared to experiments [4] and a thermodynamic assessment [6].Results are shown for the best converged supercells. b) The free energy of mixing at 1100 1250 and 1500 K assuming an ideal solution.

ble in the pair distribution functions. The U-U pair distribution function for mixtures with a composition equal to or above a fractional UCl_3 concentration of 0.36 maintain the same shape and height as in pure UCl_3 (they essentially overlap), which emphasizes the importance of network formation in the mixtures. Below a fractional concentration of 0.36 the U-U pair distribution function rapidly deviates from the pure UCl_3, indicating an inability to maintain the favorable network structure. This behavior is visible in the third coordination shell in Figure 11. Related changes may be observed in other distribution functions. The location of this transition coincides with the minimum in the mixing energy and the maximum deviation of the density from an ideal solution (compare Figures 11, 7 and 10). In turn, these coincide with the eutectic composition according to the experimental phase diagram [6]. Combined with the evolution of the U-Cl and U-U pair distribution functions in the mixtures, this suggests that the negative mixing energy is driven by increases in the Cl coordination around U ions, but if the fractional UCl_3 concentration is below ≈ 0.36, the gain from increasing this U-Cl coordination is countered by not being able to maintain the favorable U-U coordination seen in UCl_3, as evidenced by the break-up of the network structure. The balance of the increase in the U-Cl coordination and decrease in U-U coordination as function of the composition of NaCl-UCl_3 salts is responsible for the minimum in the mixing energy and by extension the location of the eutectic point in the phase diagram.

The negative deviation from an ideal solution exhibited by the density implies that the volume increases. Often, a negative mixing energy is associated with a stronger bonding and lower volume, clearly that is opposite to what is observed

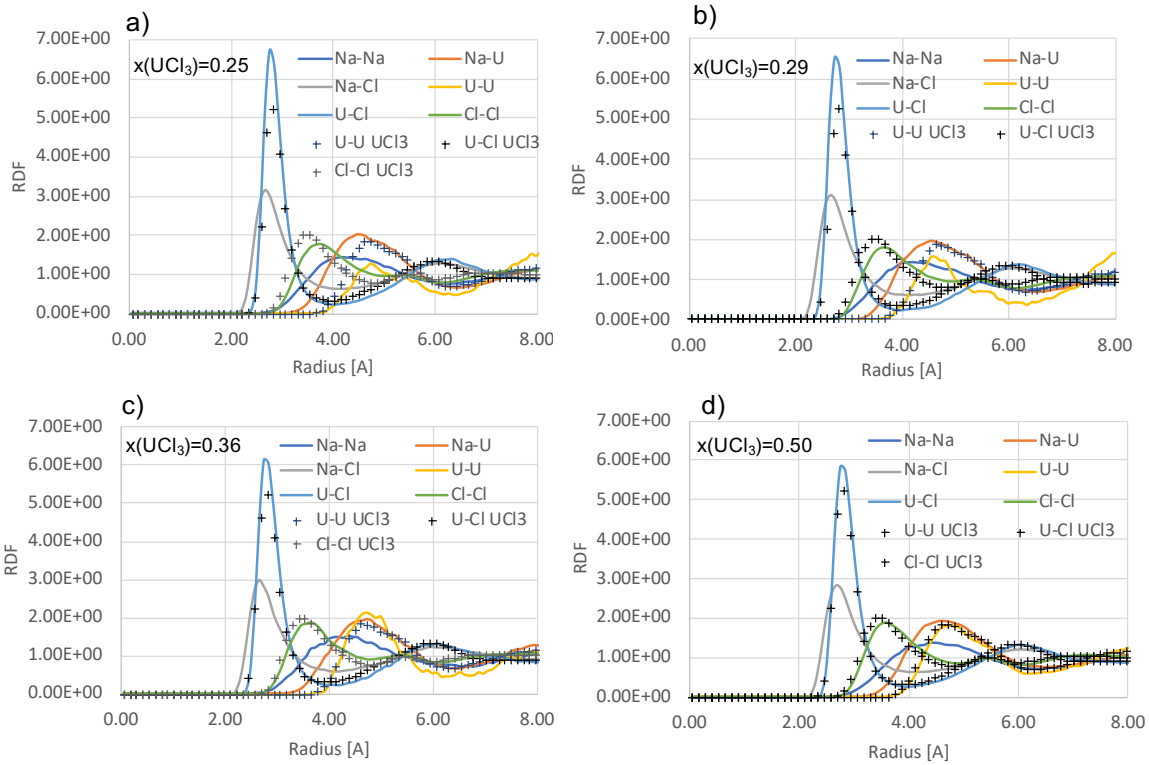

Figure 11: Pair distribution functions for NaCl-UCl_3 mixtures as function of composition ($x = 0.25$, $x = 0.29$, $x = 0.36$ and $x = 0.50$). The reference U-Cl and U-U pair distribution functions for UCl_3 are plotted in each figure for comparison.

for NaCl-UCl_3. The reason for increased volume and decreased density is again related to the evolution of the pair distribution function. The increased coordination number of Cl around U ions means that the bonding environment starts to resemble that of U^{4+} ions in UCl_4, which may also be what drives the favorable interaction. The density of UCl_4 is noticeably lower (and the molar volume higher) than that of UCl_3, which we believe correlates with the negative deviation form an ideal mixture for the density of NaCl-UCl_3 mixtures. Note that this analogy does not imply presence of formal U^4+ ions in NaCl-UCl_3, but a partial transition that drives the evolution of both the mixing energy and density. Additional simulations and experiments would be required to prove this hypothesis. What we can say is that the higher U^{3+}-Cl^- coordination in the mixed salts leads to an increase in volume and a corresponding decrease in the density.

5. Summary and conclusions

Development of next-generation molten salt reactors (MSRs) require accurate thermodynamic and thermophysical properties of fuel-bearing salt mixtures and how those change with composition as well as with addition of corrosion and fission products. The challenges associated with handling radioactive and corrosive salts make experimental measurements challenging. Using atomic scale simulations to fill these data gaps and to provide mechanistic understanding of property relations would facilitate more accurate evaluation of various concepts by reactor designers, developers and other interested parties. Modeling and simulations have an important role to play in reducing data gaps, because the compositional space of interest is extensive and difficult to cover with experiments alone, especially since some of the salts are also highly toxic or radioactive.

Following this recipe, AIMD simulations relying on different models for Van der Waals interactions were used to predict temperature dependent ther-

mophysical (density and thermal expansion) and thermodynamic (mixing energy and heat capacity) properties of NaCl mixed with UCl_3. Further details to be added. AIMD simulations of the pure end-member systems are able to accurately reproduce experimental data on densities and heat capacities provided that Van der Wals interactions are included in the simulations. The best agreement is obtained for the dDsC correlation. Further details to be added. Mixtures of UCl_3 with NaCl exhibit a negative mixing energy, with a minimum close to the eutectic composition of $x = 0.35$. For NaCl-UCl_3 the mixing energy is predicted to be independent of temperature. The predicted mixing energy for NaCl-UCl_3 agree very well with available experimental data. The existence of a minimum for mixing energy is related to the evolution of the radial distribution function. Addition of NaCl to UCl_3 increases the U-Cl coordination, which is a favorable reaction. Up until $x = 0.35$ the system is able to increase this coordination number, while maintaining the intermediate range U-U correlation. This behavior is a consequence of the tendency of UCl_3 to form network structures. For a UCl_3 fraction less than approximately 0.35, the U-U coordination starts to decrease and deviate from pure UCl_3, which leads to a lower mixing energy (less favorable). The $x = 0.35$ composition coincides with the observed eutectic composition. The same interactions that control the mixing energy also govern the evolution of the density for mixed salts. NaCl-UCl_3 exhibits a maximum deviation from ideal solution behavior at $x = 0.35$. The densities of the mixed salts are lower than for the ideal mixture. The maximum deviation is about 2% for NaCl-UCl_3 and 3% for KCl-UCl_3. The maximum deviation is only weakly dependent on temperature, but the deviation from ideal solution behavior exhibits some temperature dependence in the UCl_3 rich range. The predicted densities for the mixed systems agree at least qualitatively with available experimental data. New experiments would be required to assess the quantitive accuracy of the simulations.

Acknowledgements

This work was funded by the U.S. Department of Energy (DOE), Office of Nuclear Energy, Nuclear Energy Advanced Modeling and Simulation (NEAMS) program. Los Alamos National Laboratory, an affirmative action/equal opportunity employer, is operated by Triad National Security LLC, for the National Nuclear Security Administration of the U.S. Department of Energy under Contract No. 89233218CNA000001. Los Alamos Laboratory Directed Research and Development (LDRD) is acknowledged for supporting method development and establishing simulations procedures used in part of this study.

[1] P. N. Haubenreich, J. R.Engel, Experience with the molten-salt reactor experiment, Nuc. Appl. Technol. 8 (1970) 118.

[2] G. J. Janz, Thermodynamic and transport properties for molten salts: Correlation equations for critically evaluated density, surface tension, electrical conductance, and viscosity data, J. Phys. Chem. Ref. Data 17 (1988) 1 – 309.

[3] V. N. Desyatnik, S. F. Katyshev, S. P. Raspopin, Y. F. Chervinskii, Density, surface tension, and viscosity of uranium trichloride-sodium chloride melts, Sov. At. Energy 39 (1975) 649.

[4] H. Matsuura, R. Takagi, L. Rycerz, M. Gaune-Escard, Enthalpies of mixing in molten UCl_3-NaCl system, J. Nucl. Sci. Technol. 39 (sup3) (2002) 632–634.

[5] O. Benes, R. J. M. Konings, Thermodynamic evaluation of the NaCl-$MgCl_2$-UCl_3-$PuCl_3$ system, J. Nucl. Mater. 375 (2) (2008) 202–208.

[6] H. Yin, J. Lin, B. Hu, W. Liu, X. Guo, Q. Liu, Z. Tang, Thermodynamic description of the constitutive binaries of the NaCl-Cl-UCl_3-$PuCl_3$ system, Calphad 70 (2020) 101783.

[7] B. Li, S. Dai, D.-E. Jiang, First-principles molecular dynamics simulations of UCl_n-NaCl (n = 3, 4) molten salts, ACS Appl. Energy Mater. 2 (2019) 2122.

[8] B. Li, S. Dai, D. en Jiang, Molecular dynamics simulations of structural and transport properties of molten NaCl-UCl_3 using the polarizable-ion model, J. Mo. Liq. 299 (2020) 112184.

[9] H. O. Nam, D. Morgan, Redox condition in molten salts and solute behavior: A first-principles molecular dynamics study, J. Nucl. Mater. 465 (2015) 224.

[10] J. Song, S. Shi, X. Li, L. Yan, First-principles molecular dynamics modeling of UCl_3 in LiCl-KCl eutectic, J. Mol. Liq. 234 (2017) 279–286.

[11] G. Kresse, J. Furthmuller, Efficient iterative schemes for ab initio total-energy calculations using a plane-wave basis set, Phys. Rev. B 54 (1996) 11169–11186.

[12] G. Kresse, D. Joubert, From ultrasoft pseudopotentials to the projector augmented-wave method, Phys. Rev. B 59 (1999) 1758–1775.

[13] P. E. Blöchl, Projector augmented-wave method, Phys. Rev. B 50 (1994) 17953–17979.

[14] A. I. Liechtenstein, V. I. Anisimov, J. Zaanen, Density-functional theory and strong interactions: Orbital ordering in mott-hubbard insulators, Phys. Rev. B 52 (1995) R5467–R5470.

[15] M. Cococcioni, S. de Gironcoli, Linear response approach to the calculation of the effective interaction parameters in the LDA + U method, Phys. Rev. B 71 (2005) 035105.

[16] S. L. Dudarev, D. N. Manh, A. P. Sutton, Effect of mott-hubbard correlations on the electronic structure and structural stability of uranium dioxide, Philos. Mag. B 75 (5) (1997) 613–628.

[17] H. O. Nam, A. Bengtson, K. Vörtler, S. Saha, R. Sakidja, D. Morgan, First-principles molecular dynamics modeling of the molten fluoride salt with Cr solute, J. Nucl. Mater. 449 (2014) 148.
[18] S. Grimme, S. Ehrlich, L. Goerigk, Effect of the damping function in dispersion corrected density functional theory, J. Comp. Chem. 32 (7) (2011) 1456–1465.
[19] M. Dion, H. Rydberg, E. Schröder, D. C. Langreth, B. I. Lundqvist, Van der waals density functional for general geometries, Phys. Rev. Lett. 92 (2004) 246401.
[20] J. ří Klimeš, D. R. Bowler, A. Michaelides, Van der waals density functionals applied to solids, Phys. Rev. B 83 (2011) 195131.
[21] S. N. Steinmann, C. Corminboeuf, Comprehensive benchmarking of a density-dependent dispersion correction, J. Chem. Theory Comput. 7 (2011) 3567 – 3577.
[22] S. N. Steinmann, C. Corminboeuf, A generalized-gradient approximation exchange hole model for dispersion coefficients, The Journal of Chemical Physics 134 (4) (2011) 044117.
[23] H. Kim, J.-M. Choi, W. A. Goddard, Universal correction of density functional theory to include london dispersion (up to lr, element 103), J. Phys. Chem. Lett. 3 (3) (2012) 360–363.
[24] F. G. Edwards, J. E. Enderby, R. A. Howe, D. I. Page, The structure of molten sodium chloride, J. Phys., C, Solid State Phys. 8 (21) (1975) 3483–3490.
[25] Nist chemistry web book (2013).
URL `http://webbook.nist.gov/chemistry/`
[26] G. W. Neilson, A. K. Adya, S. Ansell, 8 neutron and x-ray diffraction studies on complex liquids, Annu. Rep. Prog. Chem., Sect. C: Phys. Chem. 98 (2002) 273–322.
[27] Y. Okamoto, F. Kobayashi, T. Ogawa, Structure and dynamic properties of molten uranium trichloride, J. Alloy. Compd. 29 (1998) 355–358.